

## SYNTHESIS, CHARACTERIZATION AND EVALUATION OF FERROELECTRIC AND DIELECTRIC BEHAVIOR OF Ni-DOPED $\text{Ba}_{0.7}\text{Sr}_{0.3}\text{TiO}_3$ THIN FILMS PREPARED VIA SOL-GEL ROUTE

M. Y. SHAHID<sup>a\*</sup>, M. N. RASHEED<sup>a</sup>, K. FATIMA<sup>a</sup>, A. MARYAM<sup>a</sup>, F. MALIK<sup>a</sup>  
M. ASGHAR<sup>a</sup>, M. F. WARSI<sup>b</sup>

<sup>a</sup>*Department of Physics, The Islamia University of Bahawalpur, Bahawalpur-63100, Pakistan*

<sup>b</sup>*Department of Chemistry, The Islamia University of Bahawalpur, Bahawalpur-63100, Pakistan*

$\text{BaSrTiO}_3$  thin films doped with transition metal  $\text{Ni}^{2+}$  ions with compositional formula  $\text{Ba}_{0.7}\text{Sr}_{0.3}\text{Ti}_{1-x}\text{Ni}_x\text{O}_3$  ( $x = 0.0, 0.1, 0.5$  and  $1.0$  mol %) were synthesized via sol-gel process. Films were deposited on Ti-substrate by spin coating technique. As-prepared films were dried at  $100^\circ\text{C}$  in air atmosphere and then annealed at  $750^\circ\text{C}$  for 2-hrs. The annealed films were investigated by different characterization methods. Among these are x-ray diffraction (XRD), scanning electron microscope (SEM), electron probe micro-analyzer (EPMA), ferroelectric characteristics, electrochemical response and dielectric properties. The XRD patterns of  $\text{BaSrTiNiO}_3$  (BSTN) samples confirmed the lattice parameters and the tetragonal phase crystal structure. It has been observed that there is no phase change in the crystal structure because of Ni-doping. The SEM micrographs present the progress of crystal phase in surface morphology of films. It is also observed that the cracks in the surface of the films decrease with  $\text{Ni}^{2+}$  ions incorporation. The EPMA results confirm the sample compositions. The room temperature P-V hysteresis loops measurements display that the remnant polarization increases with the increase in the dopant concentration. The electrochemical measurements of BSTN thin films show the change in the current density (J) with the working potential (v). The dielectric characteristics as a function of frequency within the range of values from 10 KHz to 10 MHz of the prepared films were carried out at the ambient temperature. It has been observed that the dielectric constant ( $\epsilon_r$ ) decreases initially with increasing the frequency and then remains almost constant at higher frequency (1 MHz-10 MHz). It is also observed that ' $\epsilon_r$ ' increases with the  $\text{Ni}^{2+}$  incorporation. The dielectric constant ( $\epsilon_r$ ) has the maximum value  $3.1 \times 10^{-3}$  at 10MHz frequency for the  $\text{Ba}_{0.7}\text{Sr}_{0.3}\text{NiO}_3$  film composition. The dominating effect of doping on electrical, ferroelectric and dielectric properties is greatly encouraging for the fabrication of devices operating at high frequencies.

(Received October 18; 2017; Accepted December 14, 2017)

**Keywords:** Barium strontium titanate (BST), Thin film, Sol-Gel, XRD, SEM, Ferroelectric and Dielectric properties.

### 1. Introduction

In the recent decades, Barium strontium titanate (BST), a ferroelectric as well as a dielectric material, is being used extensively for many applications like phased array devices, thin film capacitors, dynamic random access memories (DRAM) and tunable ferroelectric microwave devices. Because of the enormous applications in modern technologies, the interest to investigate the BST material has been increased. A dielectric material is an electrical insulator and it can be polarized by the application of an electric field. The study of dielectric properties of a material is concerned with the dissipation and storage of electric and magnetic energy in the material. Dielectrics are very important for clarifying different phenomena in solid-state physics, electronics

---

\*Corresponding author: mys\_sec@hotmail.com

and optics. Dielectric materials with good features are the need of the time [1, 2]. BST is a ternary compound with the stoichiometric formula  $\text{Ba}_{1-x}\text{Sr}_x\text{TiO}_3$ . It possesses relatively high dielectric constant, low dielectric loss and minute breakdown field strength. Due to these features, it is a strong candidate for DRAM applications [3]. The  $\text{Ta}_2\text{O}_5$  and  $\text{SiO}_2$  are some conventional dielectric materials whose effective oxide thickness (EOT) is low and as a consequence produce high leakage current films. But BST has high EOT and it can be anticipated that BST will be a substitute of the conventional dielectric materials for providing high charge storage capacity [4]. The dielectric characteristics of a ferroelectric material mostly depend upon the composition of the material, thickness of the film, type of doping material, film geometry, interfacial quality and deposition technique [5]. The crystal structure of BST is an  $\text{ABO}_3$  perovskite and the addition of acceptor or donor dopants is the best way to differ the material properties [6]. The ferroelectric properties of BST perovskite structure can be strongly managed by doping with different elements. A lot of studies have been reported on various types of dopants like  $\text{Ni}^{2+}$ ,  $\text{Mg}^{2+}$ ,  $\text{Fe}^{2+}$ ,  $\text{Fe}^{3+}$ ,  $\text{Mn}^{2+}$ ,  $\text{Mn}^{3+}$ ,  $\text{Al}^{3+}$ ,  $\text{Co}^{2+}$ ,  $\text{Co}^{3+}$  that have been used to change the perovskite structure of BST and as a result the leakage current density and dielectric loss are reduced [7, 8].  $\text{Ba}_{0.5}\text{Sr}_{0.5}\text{TiO}_3$  ceramics doped with nickel oxide were prepared via solid state reaction method and it was resulted that nickel ( $\text{Ni}^{2+}$ ) doped BST showed very good dielectric properties such as enhanced dielectric constant while retaining a proper charge storage capacitance [9]. However, the effect of  $\text{Ni}^{2+}$  dopant on various compositions of BST was not completely tested. In another study, it was mentioned that  $\text{Ni}^{2+}$  doped  $\text{Ba}_{0.6}\text{Sr}_{0.4}\text{TiO}_3$  ceramics grown by usual mixed oxide process revealed the increase in leakage current [10]. In recent years,  $\text{Ni}^{2+}$  doped  $\text{Ba}_{0.6}\text{Sr}_{0.4}\text{TiO}_3$  ceramics were synthesized by sol-gel technique and it was observed that the structural and optical properties were highly altered due to the dopant inclusion [11]. On the basis of literature survey, the dielectric and ferroelectric properties of sol-gel derived  $\text{Ni}^{2+}$  substituted  $\text{Ba}_{0.7}\text{Sr}_{0.3}\text{TiO}_3$  thin films have not been explored yet for the electronic and optoelectronic applications. Several methods have been used to prepare the  $\text{BaSrTiO}_3$  (BST) thin films. Among these methods, hydrothermal process, solid-state reaction method, precipitation technique, sol-gel method and spray pyrolysis process are widely used [12, 13].

In the present study, we have used the sol-gel route for the fabrication of  $\text{Ni}^{2+}$  incorporated  $\text{Ba}_{0.7}\text{Sr}_{0.3}\text{Ti}_{1-x}\text{Ni}_x\text{O}_3$  films. The choice of sol-gel process for the growth of efficient thin films was preferred due to its simple, easy and cost effective approach. Also such growing method is widely used for the preparation of BST powder as well as thin films. The main purpose of this study is to investigate the effect of  $\text{Ni}^{2+}$  addition on the dielectric and ferroelectric characteristics of a range of compositions of  $\text{BaSrTiO}_3$  thin films.

## 2. Experimental details

Thin films of barium strontium titanate,  $\text{Ba}_{0.7}\text{Sr}_{0.3}\text{Ti}_{1-x}\text{Ni}_x\text{O}_3$ , with different Ni-dopant concentration were grown using the sol-gel method. The initial materials used were barium acetate ( $\text{Ba}(\text{C}_2\text{H}_3\text{O}_2)_2$ ), strontium acetate ( $\text{Sr}(\text{CH}_3\text{COO})_2$ ), titanium (iv) n-butoxide ( $\text{Ti}(\text{C}_{16}\text{H}_{36}\text{O}_4)$ ) and Nickel (ii) acetate ( $\text{Ni}(\text{CH}_3\text{COO})_2 \cdot 2\text{H}_2\text{O}$ ). These materials were weighed according to the sample composition and then mixed uniformly in aqueous phases to obtain the homogeneous compositions. Barium acetate, strontium acetate and nickel (ii) acetate were dissolved in heated glacial acetic acid separately and then stirred till to obtain a clear solution. These three solutions were mixed together to form a nickel incorporated barium strontium complex solution. A stoichiometric proportions of titanium (iv) n-butoxide was dissolved in 2-methoxyethanol and then added it to the complex solution with continuous stirring at  $80^\circ\text{C}$ . Finally, a small amount of ethylene glycol was added for stability of the solution. The resulting solution was stirred continuously for 1h. It was a stock solution of  $\text{BaSrTiNiO}_3$  (BSTN) that was used for spin coating on titanium (Ti) substrates. Ti- substrates were cleaned with acetone, isopropanol (IPA) and deionized water at  $80^\circ\text{C}$  for 10-minutes sequentially and after that the thin film was deposited by spin coating process. Each thin film consists of three layers and every layer was subjected to a controlled heat treatment cycle in a rapid thermal process. Spin coated layer was calcined at  $100^\circ\text{C}$  for 10-minutes in a muffle furnace, in this way a thin film was made by three layers. Lastly, the

whole film was annealed at 750 °C for 2-hrs in air atmosphere. The materials used in the synthesis of the samples for different compositions are given in table 1.

Table 1. The amount of different materials used in the synthesis of various compositions of  $Ba_{0.7}Sr_{0.3}Ti_{1-x}Ni_xO_3$  samples.

Sr. No.	Materials name	X=0.0M	X=0.1M	X=0.5M	X=1.0M
1	Barium acetate ( $Ba(C_2H_3O_2)_2$ ) in g	2.682	2.682	2.682	2.682
2	Strontium acetate ( $Sr(CH_3COO)_2$ )	0.956 g	0.956 g	0.956 g	0.956 g
3	Titanium (iv) n-butoxide ( $Ti(C_{16}H_{36}O_4)$ ) ( $dm^3$ )	$5.26 \times 10^{-3}$	$4.74 \times 10^{-3}$	$2.63 \times 10^{-3}$	0.00
4	Nickel (ii) acetate ( $Ni(CH_3COO)_2 \cdot 2H_2O$ ) in g	0.00	0.266	1.326	2.652
5	Glacial acetic acid ( $dm^3$ )	$1.5 \times 10^{-2}$	$1.5 \times 10^{-2}$	$1.5 \times 10^{-2}$	$1.5 \times 10^{-2}$
6	Ethylene glycol ( $dm^3$ )	$5.0 \times 10^{-3}$	$5.0 \times 10^{-3}$	$5.0 \times 10^{-3}$	$5.0 \times 10^{-3}$
7	2-methoxyethanol ( $dm^3$ )	$1.5 \times 10^{-2}$	$1.5 \times 10^{-2}$	$1.5 \times 10^{-2}$	$1.5 \times 10^{-2}$

X-ray diffraction (XRD, X'Pert Pro PW 3040 Panalytical, Almelo, and the Netherlands) was used to study the structural phases and to observe the phase formation of BSTN thin films with different  $Ni^{2+}$  concentration. XRD was done using  $CuK\alpha$  as a radiation source with wavelength ( $\lambda = 1.54056 \text{ \AA}$ ). XRD plots were obtained by varying the diffraction angle ( $2\theta$ ) from 20 to 60°. Surface morphology of the BSTN films was characterized by scanning electron microscopy (SEM). The compositional analysis of the samples was done at different spots using electron probe micro-analyzer (EPMA). Hewlett-Packard 4275A multi-frequency LCR meter with 16047A test fixture was used to investigate the dielectric properties of BSTN films. A modified Sawyer Tower circuit was used to perform the polarization-working voltage (P-V) hysteresis loop measurements of the samples. The flow chart about the experimental arrangement is given in Fig. 1.

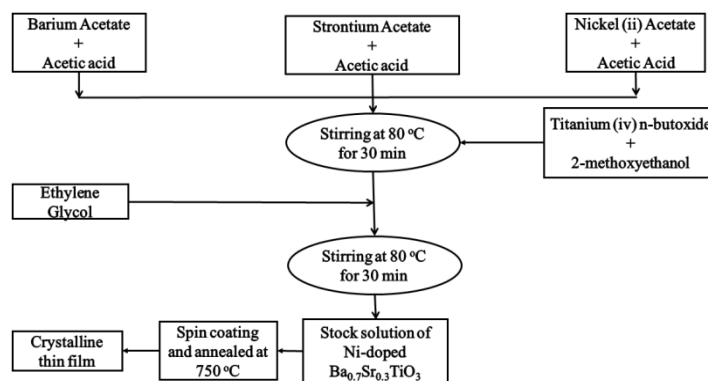


Fig. 1. Flow chart showing the different steps taken in the synthesis of  $Ba_{0.7}Sr_{0.3}Ti_{1-x}Ni_x$  films

### 3. Results and discussions

#### 3.1 X-ray diffraction (XRD)

The XRD patterns of pure and doped  $\text{Ba}_{0.7}\text{Sr}_{0.3}\text{Ti}_{1-x}\text{Ni}_x\text{O}_3$  thin films are shown in Fig. 2.

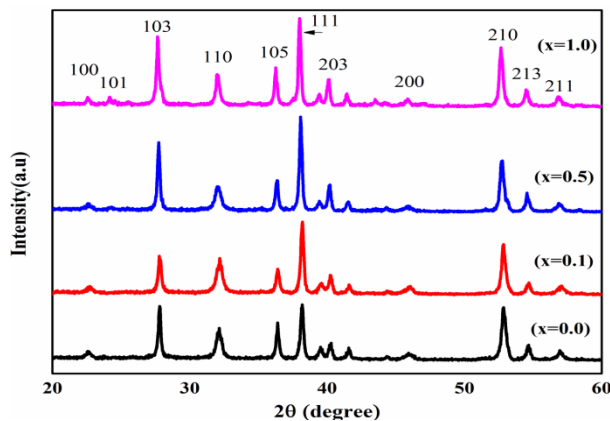


Fig. 2. XRD plots of sol-gel synthesized un-doped and  $\text{Ni}^{2+}$  doped  $\text{Ba}_{0.7}\text{Sr}_{0.3}\text{Ti}_{1-x}\text{Ni}_x\text{O}_3$  thin films

All the XRD plots depict the sharp and visible peaks that confirm the crystalline structure and the phase pattern in the grown samples. The XRD measurements show that all the grown samples have tetragonal phase structure. The lattice parameters and hkl of the selected peaks at different diffraction angles ( $2\theta$ ) are tabulated in the Table 2 [14].

Table 2. The lattice constants, angle ( $2\theta$ ) and hkl of the selected peaks for tetragonal phase structure of  $\text{Ba}_{0.7}\text{Sr}_{0.3}\text{Ti}_{1-x}\text{Ni}_x\text{O}_3$  films

Concentration	X = 0.0	X = 0.1	X = 0.5	X = 1.0
hkl	$2\theta$	$2\theta$	$2\theta$	$2\theta$
100	22.5985	22.6501	22.5985	22.5962
101	23.8256	23.8256	24.2896	24.1659
103	27.7750	27.7750	27.7750	27.6146
110	32.1987	32.1987	32.1059	32.0037
105	36.4368	36.4368	36.3440	36.2993
111	38.2207	38.2207	38.0351	37.9720
203	40.2933	40.2933	40.2005	40.0573
200	45.9441	46.0369	45.9441	45.8203
210	52.9148	52.9148	52.7188	52.7177
213	54.6987	54.6987	54.6059	54.4935
211	56.9569	57.0187	56.8641	56.8996
Lattice constant a(Å)	3.78942	3.789428	3.80222	3.806764
Lattice constant c(Å)	16.39769	16.39769	16.40276	16.46218
c(Å) / a(Å)	4.327220	4.327220	4.313996	4.324455

These results show that  $\text{Ni}^{2+}$  doping in BST increases the cell parameters; it may be due to replacement of smaller ionic radii of  $\text{Ti}^{4+}$  ion by larger ionic radii of  $\text{Ni}^{2+}$ . It is observed that with the increase in doping content, the phase of growing samples remains unchanged but a slight shift is noticed in the XRD peaks. Therefore, it can be concluded that the nickel addition cannot alter the BST structure. The shift in peaks (noticed at peak [210]) could be explained on the basis of the expansion in the crystal lattice. As the ionic radii of  $\text{Ni}^{2+}$  (0.69 Å) and  $\text{Ti}^{4+}$  (0.61 Å) are much closer to each other while the ionic radii of  $\text{Ba}^{2+}$  (1.36 Å) are larger than the ionic radii of  $\text{Ni}^{2+}$  and  $\text{Ti}^{4+}$ , hence it is expected that  $\text{Ni}^{2+}$  ions replace the B site of  $\text{ABO}_3$  perovskite structure. As the ionic radii of  $\text{Ni}^{2+}$  are somewhat larger than  $\text{Ti}^{4+}$ , hence the addition of  $\text{Ni}^{2+}$  ions may cause the expansion of crystal lattice and the increase in the oxygen vacancies along with the decrease in the electrons. As a result the leakage current densities in BST films can be reduced considerably due to this low electron density [15]. Fig. 2 presents that the peaks intensity of plot for  $x = 1.0$  is higher than that of plots for  $x = 0.1$  and  $x = 0.5$  concentration. The samples with higher doping concentration show the sharper of the XRD peaks and therefore, it can be resulted that higher concentration of dopant material improve the crystal structure of BSTN thin films.

### 3.2 Scanning electron microscope (SEM)

The SEM images of pure and doped BSTN thin films are shown in Fig. 3. These SEM micrographs show that the addition of  $\text{Ni}^{2+}$  greatly improves the crystallinity as well as decreases cracks in the surface of the films. Fig. 3 (a) reveals that the un-doped  $\text{Ba}_{0.7}\text{Sr}_{0.3}\text{TiO}_3$  thin films have large surface cracks while Fig. 3 (b, c & d) displays that  $\text{Ni}^{2+}$  doped  $\text{Ba}_{0.7}\text{Sr}_{0.3}\text{Ti}_{1-x}\text{Ni}_x\text{O}_3$  films have less or nearly no cracks with a uniform and homogeneous surface. Hence it is concluded that the doping material strongly affect the surface morphology of thin films. A similar behavior has been reported for MOD prepared BST thin films [16].

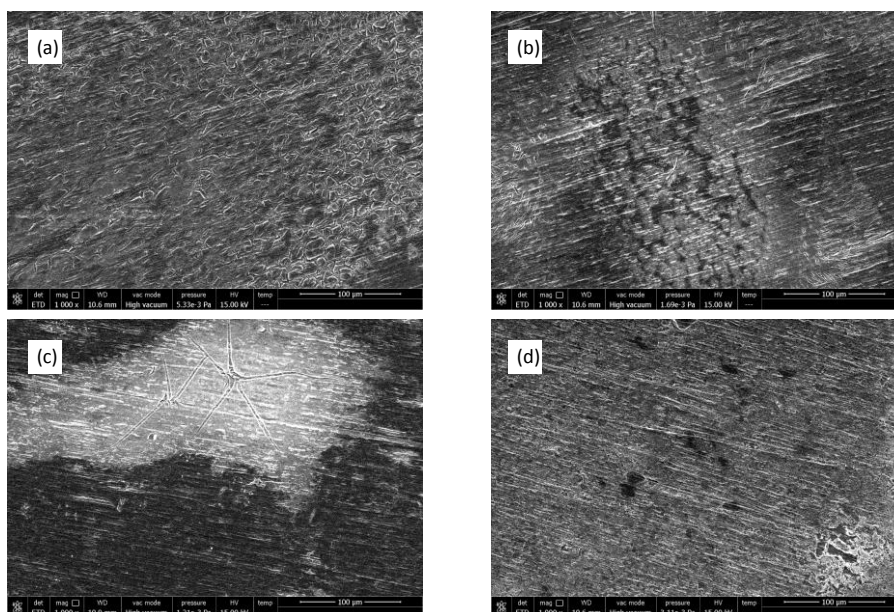


Fig.3. SEM images of pure and nickel-doped  $\text{Ba}_{0.7}\text{Sr}_{0.3}\text{Ti}_{1-x}\text{Ni}_x\text{O}_3$  thin films (a)  $x = 0.0$  mol%, (b)  $x = 0.1$  mol%, (c)  $x = 0.5$  mol% and (d)  $x = 1.0$  mol%.

### 3.3 Electron probe micro analyzer (EPMA)

Table 3 summarizes the electron probe micro analyzer (EPMA) results of the samples composition analysis of pure and Ni-doped  $\text{Ba}_{0.7}\text{Sr}_{0.3}\text{TiO}_3$  films. This novel technique has some advantages over the other surface analysis methods especially when it deals to multi-component metal oxides. EPMA results verify the elemental compositions of the grown samples that were used in this experiment.

Table 3. EPMA data of sample composition analysis of pure and nickel-doped  $Ba_{0.7}Sr_{0.3}Ti_{1-x}Ni_xO_3$  thin films in molar percent

Composition	Ba (%)	Ti (%)	Sr (%)	Ni (%)	Cl (%)
$Ba_{0.7}Sr_{0.3}TiO_3$	35.1698	50.2925	14.4282	---	0.1095
$Ba_{0.7}Sr_{0.3}Ti_{0.9}Ni_{0.1}O_3$	35.6672	46.0105	12.5714	5.7510	---
$Ba_{0.7}Sr_{0.3}Ti_{0.5}Ni_{0.5}O_3$	34.7580	24.6772	11.5245	29.0258	0.0144
$Ba_{0.7}Sr_{0.3}NiO_3$	32.5435	---	11.5393	52.1131	3.8041

### 3.4 Ferroelectric measurements

To characterize the samples electrically, they were coated by a gold film of thickness 300 nm and area  $1.5 \times 1.5 \text{ cm}^2$  using thermal evaporating system. As a result our samples are in the configuration of metal-ferroelectric-metal pattern. Fig. 4 shows the room temperature polarization vs applied voltage (P-V) hysteresis curves for the various compositions of  $Ba_{0.7}Sr_{0.3}Ti_{1-x}Ni_xO_3$  films. These plots reveal that the value of maximum polarization and the shape of the hysteresis curves mainly depend on  $Ni^{2+}$  concentration. The value of remnant polarization of films increases with the increase of doping content. A number of the films display the narrow ferroelectric hysteresis loops, while a well defined loop is achieved from  $Ba_{0.7}Sr_{0.3}NiO_3$  sample because of high  $Ni^{2+}$  concentration and surface homogeneity. It is also observed that the loops expose cycle broadness that increases with increasing the Ni-doping concentration. Therefore, it is concluded that ferroelectric behavior of  $Ba_{0.7}Sr_{0.3}Ti_{1-x}Ni_xO_3$  films is mostly dependent on the Ni-content and homogeneity of the film surface [17-19].

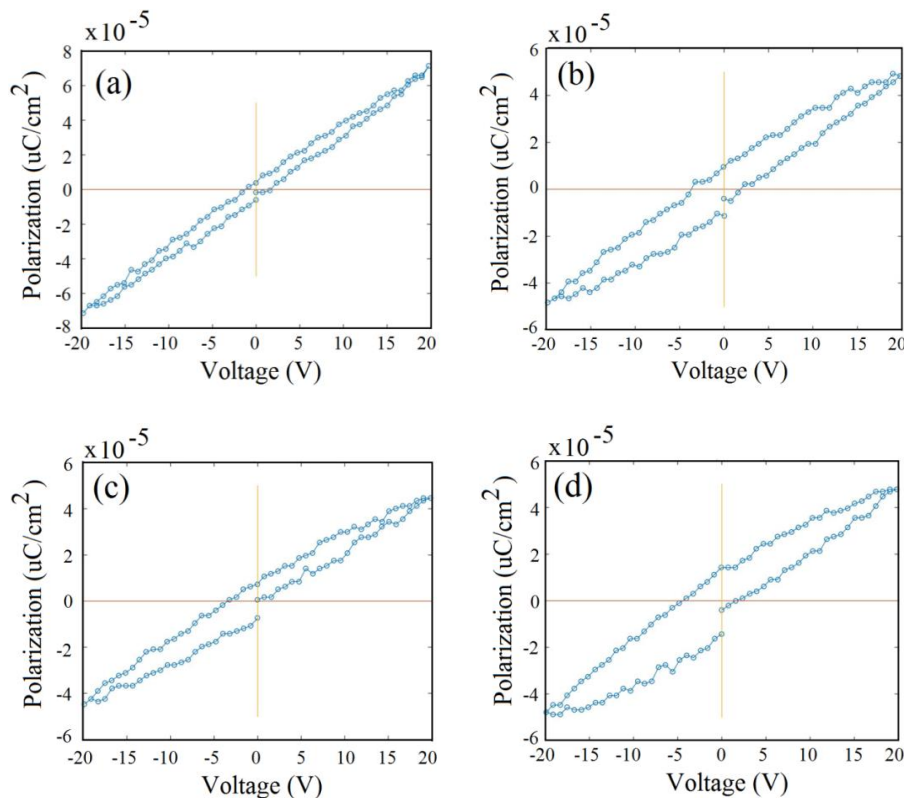


Fig. 4. Polarization vs applied voltage (P-V) hysteresis measurements of pure and nickel-doped  $Ba_{0.7}Sr_{0.3}Ti_{1-x}Ni_xO_3$  thin films (a)  $x = 0.0$ , (b)  $x = 0.1$ , (c)  $x = 0.5$  and (d)  $x = 1.0$  mol%.

### 3.5 Electrochemical characterization

The plots of current density vs applied potential (J vs V) of  $Ba_{0.7}Sr_{0.3}Ti_{1-x}Ni_xO_3$  thin films with a variety of  $Ni^{2+}$  content are shown in Fig. 5. As the voltage window is increased much beyond +2000V to -2000V against the standard hydrogen electrode. The evolution of oxygen or hydrogen is resulted. It is observed that the broadening of peaks is increased with the increase of  $Ni^{2+}$  concentration in  $Ba_{0.7}Sr_{0.3}Ti_{1-x}Ni_xO_3$  samples.

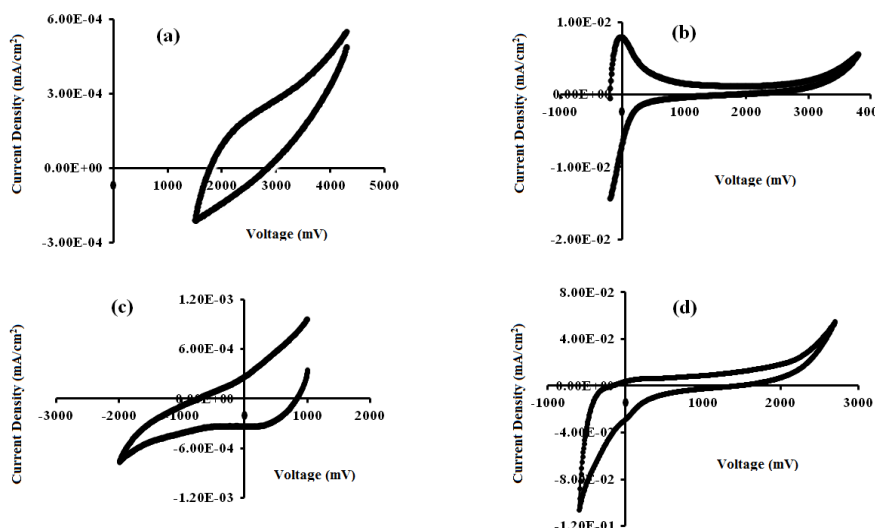


Fig. 5. Typical Cyclic voltammograms  $Ni^{2+}$  doped  $Ba_{0.7}Sr_{0.3}Ti_{1-x}Ni_xO_3$  thin films (a)  $x = 0.0$ , (b)  $x = 0.1$ , (c)  $x = 0.5$  and (d)  $x = 1.0$  mol% in  $0.05M H_2SO_4$ ,  $200mVs^{-1}$  scan rate

### 3.6 Dielectric properties measurements

The dielectric constant is a measure of the amount of polarization of the sample material. It depends on the composition, growth process and the crystal structure of the material. It is also distinct as an amount of electrostatic energy stored in a unit volume per unit potential gradient [20, 21]. The dielectric constant ( $\epsilon_r$ ) of a substance is found by the formula given below:

$$\epsilon_r = \frac{Cd}{\epsilon_o A}$$

Where 'C' the capacitance, 'd' the thickness, 'A' and ' $\epsilon_o$ ' are the surface area of the material and permittivity of free space. The room temperature dielectric constant ( $\epsilon_r$ ) vs frequency plots are given in Fig. 6.

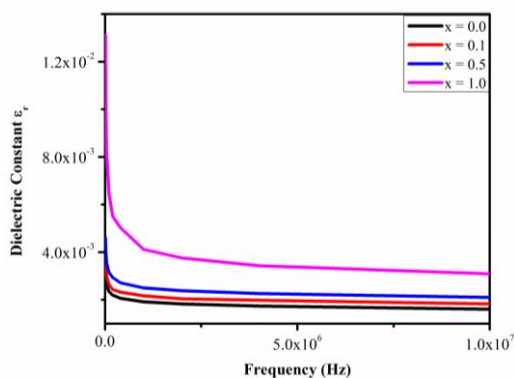


Fig. 6. Dielectric constant ( $\epsilon_r$ ) vs operating frequency ( $f$ ) of pure and nickel substituted

*Ba<sub>0.7</sub>Sr<sub>0.3</sub>Ti<sub>1-x</sub>Ni<sub>x</sub>O<sub>3</sub> thin films*

The sample with the composition Ba<sub>0.7</sub>Sr<sub>0.3</sub>NiO<sub>3</sub> (for x= 1.0) possesses the highest dielectric constant value. It is noticed that  $\epsilon_r$  increases with the increase in Ni<sup>2+</sup> concentration. The dielectric constant decreases with the operating frequency in the range of 10 KHz to 10MHz. But after 1MHz, the dielectric constant slightly reduces or almost remains constant, indicating that as-prepared BSTN thin films have stable dielectric properties in the high frequency range [14]. Table 4 shows the values of dielectric constant measured at different frequencies of pure and nickel doped Ba<sub>0.7</sub>Sr<sub>0.3</sub>Ti<sub>1-x</sub>Ni<sub>x</sub>O<sub>3</sub> films.

Table 4. Dielectric constant as a function of applied frequency of pure and Ni<sup>2+</sup> doped Ba<sub>0.7</sub>Sr<sub>0.3</sub>Ti<sub>1-x</sub>Ni<sub>x</sub>O<sub>3</sub> thin films

Frequency (MHz)	X = 0.0	X = 0.1	X = 0.5	X = 1.0
0.01	0.00361	0.00393	0.0046	0.01312
0.02	0.00299	0.00339	0.00405	0.01029
0.10	0.00235	0.00265	0.00315	0.00646
0.40	0.00206	0.00232	0.00271	0.00502
2.00	0.00182	0.00204	0.00238	0.00376
10.0	0.00161	0.00183	0.0021	0.00309

Dielectric constant vs Ni-concentration in the grown samples is plotted and shown in the Fig. 7. It is obvious from this plot that the variation of dielectric constant with Ni-concentration in the samples is about linear.

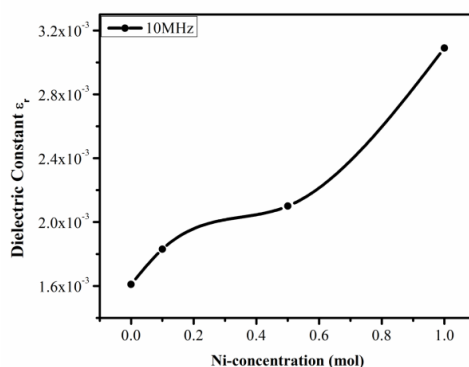


Fig. 7. Dielectric constant vs Ni-concentration (mol) of the samples.

#### 4. Conclusions

Nickel (Ni<sup>2+</sup>) substituted Ba<sub>0.7</sub>Sr<sub>0.3</sub>Ti<sub>1-x</sub>Ni<sub>x</sub>O<sub>3</sub> thin films were successfully synthesized by sol-gel process and deposited on titanium substrate through spin coating route. XRD studies confirmed its tetragonal crystalline phase structure and the average value of ratio c/a = 4.3244 were calculated through the lattice parameters. These results show that there is no change in the phase but the peak shifting is observed to the higher diffraction angle due to Ni<sup>2+</sup> doping in BaSrTiO<sub>3</sub> thin films. The SEM micrographs and the EPMA results present the homogeneous

surface morphology and confirm the elemental compositions of the prepared samples. Electrochemical, ferroelectric and dielectric properties were considerably improved due to the increase of the dopant ( $\text{Ni}^{2+}$ ) concentration in  $\text{Ba}_{0.7}\text{Sr}_{0.3}\text{Ti}_{1-x}\text{Ni}_x\text{O}_3$  films. On the basis of better characteristics, such materials have great utilization in the manufacturing of advance technological devices.

### Acknowledgements

Authors are greatly thankful to the Higher Education Commission (HEC) of Pakistan for financial support (Grant No. 2913/R&D/HE & International Research Support Initiative Program (IRSIP) grant No. 1-8/HEC/HRD/2015/3728), Center for Nanotechnology, University of Toronto, Toronto, ON, Canada and The Islamia University of Bahawalpur, Bahawalpur-63100, Pakistan.

### References

- [1] K.B. Kim, T.S. Yun, R.Y. Kim, H.S. Kim, H.G. Kim, J.C. Lee, *Microwave and optical technology letters* **45**, 15 (2005).
- [2] J. Du, K.-L. Choy, *Materials Science and Engineering: C* **26**, 1117 (2006).
- [3] M. Banerjee, S. Mukherjee, S. Maitra, *Ceramica* **58**, 99 (2012).
- [4] R. Balachandran, H. Yow, B. Ong, K.B. Tan, K. Anuar, W. Teoh, M.A. Fauzi, S. Sreekantan, V. Swaminathan, *Journal of materials science* **46**, 1806 (2011).
- [5] M. Nayak, T.-Y. Tseng, *Thin Solid Films* **408**, 194 (2002).
- [6] F. Stemme, M. Bruns, H. Geßwein, M. Schroeder, M. Sazegar, M. Drahus, R.-A. Eichel, F. Paul, C. Azucena, J. Binder, *Journal of materials science* **48**, 3586 (2013).
- [7] K.H. Yoon, J.C. Lee, J. Park, D.H. Kang, C.M. Song, Y.G. Seo, *Japanese Journal of Applied Physics* **40**, 5497 (2001).
- [8] S.-Y. Chen, H.-W. Wang, L.-C. Huang, *Japanese Journal of Applied Physics* **40**, 4974 (2001).
- [9] M.-H. Lim, H.-S. Kim, N.-Y. Kim, H.-G. Kim, I.-D. Kim, S.E. Moon, M.-H. Kwak, H.-C. Ryu, S.-J. Lee, *Journal of electroceramics* **13**, 239 (2004).
- [10] H. Seo, Y.-B. Kim, G. Lucovsky, I.-D. Kim, K.-B. Chung, H. Kobayashi, D.-K. Choi, *Journal of Applied Physics* **107**, 024109 (2010).
- [11] L. Qian, H. Deng, L. Zhu, P. Yang, J. Chu, *Journal of Physics: Conference Series*, IOP Publishing, 012183 (2011).
- [12] S. Deshpande, Y. Kholam, S. Bhoraskar, S. Date, S. Sainkar, H. Potdar, *Materials Letters* **59**, 293 (2005).
- [13] O. Thakur, C. Prakash, D. Agrawal, *Materials Letters* **56**, 970 (2002).
- [14] A.D. Kakumani, B. Ruthramurthy, H.Y. Wong, B.H. Ong, K.B. Tan, H.K. Yow, *International Journal of Applied Ceramic Technology* **13**, 177 (2016).
- [15] B.L. Cheng, T.W. Button, M. Gabbay, G. Fantozzi, M. Maglione, *Journal of the American Ceramic Society* **88**, 907 (2005).
- [16] N.A. Dhas, A. Zaban, A. Gedanken, *Chemistry of materials* **11**, 806 (1999).
- [17] B.M. Kulwicki, A. Amin, H.R. Beratan, C.M. Hanson, *Pyroelectric imaging*, IEEE, 1 (1992).
- [18] J.H. Kim, Y.S. Yoon, D.L. Polla, *Japanese Journal of Applied Physics* **37**, 948 (1998).
- [19] A. Khalfallaoui, G. Velu, L. Burgnies, J.-C. Carru, *IEEE transactions on ultrasonics, ferroelectrics, and frequency control* **57**, 1029 (2010).
- [20] M.A. Shahzad, M.F. Warsi, M.A. Khan, F. Iqbal, M. Asghar, *Journal of Alloys and Compounds* **647**, 693 (2015).
- [21] M.A. Shahzad, M. Shahid, I. Bibi, M.A. Khan, M.A. Nawaz, M.F. Aly Aboud, M. Asghar, R.N. Paracha, M.F. Warsi, (2016).